University of Plymouth

PEARL **https://pearl.plymouth.ac.uk**

Faculty of Science and Engineering School of Engineering, Computing and Mathematics

2022-07

Modelling of convection, diffusion and binding of chlorides in concrete during wetting-drying cycles

Li, L-Y

http://hdl.handle.net/10026.1/19211

10.1016/j.marstruc.2022.103240
Marine Structures
Elsevier

All content in PEARL is protected by copyright law. Author manuscripts are made available in accordance with publisher policies. Please cite only the published version using the details provided on the item record or document. In the absence of an open licence (e.g. Creative Commons), permissions for further reuse of content should be sought from the publisher or author.

To be published in "Marine Structures". https://doi.org/10.1016/j.marstruc.2022.103240.
Received 26 November 2021; Received in revise d form 23 March 2022; Accepted 5 May 2022.

Modelling of convection, diffusion and binding of chlorides in concrete during wetting-drying cycles

Dawang Li[1], Long-yuan Li[2*], Ping Li[1], Yao-cheng Wang[1*]
(1) Guangdong Provincial Key Laboratory of Durability for Marine Civil Engineering, Shenzhen University, Shenzhen 518060, P R China
(2) School of Engineering, Computing and Mathematics, University of Plymouth, Plymouth PL4 8AA, UK
(*) Corresponding authors

Abstract – Moisture convection in concrete is an important factor affecting the chloride diffusion in concrete. This paper presents a comprehensive study on the transport of moisture, carbon dioxide and chloride ions in concrete when subjected to wetting and drying cycles. A numerical model considering not only the transport of individual components but also the interaction between them is developed. The latter includes the concrete carbonation, chloride binding, the effect of concrete carbonation on chloride binding capacity, and the time-varying boundary conditions of carbon dioxide and chloride caused due to wetting and/or drying. The results obtained from the study demonstrate that when moisture convection and concrete carbonation in the convection zone near the exposed surface are involved the chloride indeed exhibits an increase in a thin layer next to exposed surface before it decreases with the distance as observed in many experiments.
Keywords – Modelling; chloride; diffusion; carbonation; wetting and drying cycles; unsaturated concrete.

1. Introduction

Chloride-induced reinforcing steel corrosion is one of the major deterioration problems in concrete structures built in marine environment. To prevent this problem, one has to know how chlorides get into concrete from its surrounding environment and how their penetration takes place in concrete medium. Numerous experimental studies have been carried out since early 1980s in order to understand the mechanism of chloride penetration in concrete and the influences of concrete mix design parameters and surrounding environment conditions on the chloride penetration. The experimental work involves the diffusion tests of chlorides in both saturated and unsaturated concretes. The latter involves both the laboratory tests of cement or concrete specimens exposed to artificial wetting and drying cycles using sodium chloride solution and field tests of directly placing cement or concrete specimens in seawater of tidal zones. For saturated concrete, the chloride concentration profiles measured from the tests can be generally described by using an error function [1] although the diffusion coefficients calculated from the best fits of experimental data may be different at different times [2],

indicating that concrete evolution may also have some influence on the penetration of chloride ions. For concrete subjected to wetting and drying cycles, however, the measured chloride concentration profiles are quite complicated. In some cases, the chloride concentration profile was found to exhibit an increase in a thin layer next to exposed surface before it decreases with increased distance [3]. So far it is still a paradox about why the maximum chloride concentration is located in the inner concrete rather than at the exposed surface when the wetting and drying cycles are involved.

Extensive research work has been carried to understand how the moisture transport affects the penetration of chloride ions in concrete. For example, Saetta et al. [4] developed a coupled numerical analysis model of moisture, heat, and chloride-ion flows through concrete. The model was used to examine the chloride diffusion in partially saturated concrete by taking into account the variability of ionic diffusion coefficients with concrete mix design parameters. Andrade et al. [5] used an analytical model of chloride diffusion to study the relative influence of concrete skin thickness on chloride penetration in concrete. Hong and Hooton [6] examined the influence of wetting and drying cycles by using sodium chloride solution on chloride ingress into concrete. Wang et al. [7] developed a transport model of ionic solution and ionic species in an unsaturated concrete by considering not only the transport of ionic species and ionic solution but also the electrostatic interaction between different ionic species. Wang et al. [8] reported an experimental study on chloride diffusion in concrete subjected to wetting and drying cycles. It was found that the highest concentration in the chloride profile was located in inner concrete not far away from the concrete surface. Zhang et al. [9] developed a mathematical model of chloride transport in concrete under wetting and drying cycles. The model considered the hysteresis of moisture evaporation and the accumulation of chlorides at concrete surface. Xu et al. [10] experimentally investigated the effect of different wetting and drying cycle conditions on the transport of chloride ions in concrete. It was found that the chloride concentration increased with increased dry-to-wet ratio; whereas the presence of convection zone under wetting and drying cycles was found to be time dependent. Arya et al. [11,12] experimentally investigated the factors affecting the surface chloride concentration, chloride binding, and chloride diffusion coefficient in concrete with supplemental cementitious materials, subjected to wetting and drying cycles. Gang et al. [13] presented a study on the effect of wetting and drying cycles on chloride transport in concrete. It was found that chloride transport accelerated in surface zone only when the drying time was longer than the wetting time in the cycles. Guan et al. [14] developed a prediction model of chloride penetration in concrete subjected to wetting and drying cycles, in which the chloride diffusion coefficient used to characterize the effect of temperature, age of concrete, humidity and wind speed on the transport of chloride ions in concrete was proposed. Lu et al. [15] presented an experimental study on chloride penetration in concrete subjected to wetting and drying cycles. They found that the convection zone depth varied from 6 mm to 15 mm. Yu et al. [16] proposed a chloride diffusion model coupled with environmental factors to describe chloride ingress into concrete. Lu et al. [17] presented an experimental investigation on chloride transport in cracked reinforced concrete beams under wetting and drying cycle conditions. Gao et al. [18] provided a statistical analysis on the convection zone depth, chloride peak value, and chloride diffusion coefficient in concrete exposed to marine tidal environment based on their field test data obtained from 270 chloride

ingress curves of tested concrete specimens. Zhang et al. [19,20] provided the time dependence and similarity analysis for chloride diffusion coefficient and chloride peak value in concrete exposed to simulated wetting and drying cycle environment. Petcherdchoo [21] proposed a set of new closed-form solutions for a linearly cyclic surface chloride function for predicting the transport of chloride ions in unsaturated concrete. Recently, Shen et al. [22] presented a numerical study on concrete carbonation and its effect on chloride binding in concrete. The work evaluated the chloride binding and subsequent ionic diffusion process in chloride-contaminated concrete caused by carbonation. Li et al. [23] investigated the combined action of carbonation and chloride ingress in concrete under stable moisture state. The chloride profile was solved analytically by using a moving boundary condition. Shen et al. [24] presented a numerical investigation on the combined action of carbonation and chloride ingress in unsaturated concrete and examined the influence of unsaturated environment on the binary ingress process of chloride and carbonation. Liang et al. [25] investigated the chloride permeability and examined the steel corrosion in concrete with carbonated recycled concrete aggregate. More recently, AL-Ameeri et al. [26] experimentally examined the potential impact of concrete carbonation on the chloride penetration, and the rate of corrosion in RC structures subjected to service-related cracks. Dang et al. [27] examined the effect of chloride ions on the durability and mechanical properties of sea-sand concrete containing supplemental cementitious materials under accelerated carbonation conditions. The results showed that the presence of chloride ions in concrete could generally improve the carbonation resistance of the concrete.

In summary, there have been extensive research works published in literature on chloride diffusion and concrete carbonation in both saturated and unsaturated concrete under wetting and drying cycle conditions. However, most of these works did not consider the interaction between chloride diffusion and concrete carbonation, particularly the influence of concrete carbonation on the chloride binding capacity of the concrete. Moreover, there is very limited work on the development of mathematical models, which are able to describe the phenomenon that chloride profile has a thin convection zone near the exposed surface where the chloride content increases with the depth, and a diffusion zone inside of the concrete where the chloride content decreases with increased depth, as observed in many experimental tests. In this paper a mathematical model is developed to describe the coupled transport mechanism of moisture, carbon dioxide, and chloride in unsaturated concrete subjected to wetting and drying cycles. The model considers not only the transport of individual components, but also the chemical reactions between them. The latter includes the moisture convection, concrete carbonation, chloride binding, and the effect of concrete carbonation on the binding capacity of chlorides and the porosity of concrete. More importantly, the study demonstrates that for unsaturated concrete the transport equations for any individual components involved have to be established based on an identical framework such as the unit volume of concrete and the corresponding boundary conditions also must be established by using the same framework.

2. Transport models of moisture, carbon dioxide and chlorides in unsaturated concrete

Concrete is a porous material. It absorbs and retains moisture because of the capillary action of

pores. When a concrete is subjected to wetting and drying cycles the moisture transport takes place in the concrete and the degree of saturation of the pore space of the concrete is dependent on its relative humidity and the previous exposure of the concrete to moisture. If the moisture content inside a concrete is less than its saturation level, water may be absorbed into the concrete by large capillary forces arising from the contact of the very small pores of concrete with the liquid phase. The concrete is referred to as a saturated concrete if the pores inside it are entirely filled with water. Otherwise, it is called unsaturated concrete if the pores are occupied by water and air. Mathematically, the moisture transport in concrete can be described using the following moisture diffusion equation [28],

$$\frac{\partial C_\theta}{\partial t} = \nabla(D_\theta \nabla C_\theta) \quad (1)$$

where C_θ is the degree of saturation, t is the time, and D_θ is the moisture diffusivity, which can be expressed as follows,

$$D_\theta = \alpha_1 C_\theta e^{\beta_1 C_\theta} \quad (2)$$

where α_1 in m^2/s and β_1 with no unit are the experimentally fitted constants. For given initial and boundary conditions of C_θ, Eq.(1) can be solved numerically and thus the degree of saturation of the concrete at any time at any place can be determined.

Concrete carbonation may take place when the concrete is subjected to wetting and drying cycles, in which carbon dioxide, CO_2, from the air outside of the concrete diffuses into concrete through gaseous and liquid phases of concrete pores and dissolves into pore solution and then, reacts with the dissolved hydration product, $Ca(OH)_2$, to form insoluble calcium carbonate, $CaCO_3$ and water [29] because the solubility of calcium carbonate (9.90×10^{-9}) is much lower than that of calcium hydroxide (9.95×10^{-4}). The detailed description of the concrete carbonation can be found in the work of Bary and Sellier [30]. Note that the gaseous CO_2 cannot directly react with the hydrates of the cement paste. It must first dissolve in water to form carbonate ions and then reacts with Ca ions in the pore solution. Since, in general, the reaction between carbonate ions and calcium ions in pore solution is much quicker than the diffusion of the CO_2 in concrete, the reaction can be assumed to take place only at the carbonation front, whereas the transport of CO_2 can be assumed to take place only in the gaseous phase as CO_2 diffusion is much quicker in gaseous phase than in liquid phase. The consumption of CO_2 in the carbonation front can be assumed to be controlled by the availability of $Ca(OH)_2$ or calcium ions in the pore solution. Under these assumptions, the chemical reactions involved in the concrete carbonation can be simplified as follows,

$$Ca(OH)_2(s \rightarrow aq) + CO_2(g \rightarrow aq) \rightarrow CaCO_3(s) + H_2O(aq) \quad (3)$$

where the dissolved $Ca(OH)_2$ in pore solution will quickly decompose into calcium ions and hydroxide ions. Thus, Eq.(3) can be also expressed as follows,

$$Ca^{2+}(aq) + 2OH^-(aq) + CO_2(aq) \rightarrow CaCO_3(s) + H_2O(aq) \quad (4)$$

The transport of CO_2 in concrete gaseous phase can be described by using Fick laws with considering the consumption of CO_2 at the carbonation front, whereas the transport of calcium and hydroxide ions and the liquid water generated during the carbonation process can be generally ignored [31,32]. In this case, the mass conservation equation of CO_2 considered in per-unit volume of concrete can be expressed as follows,

$$\frac{\partial C_{CO2}}{\partial t} = \nabla\left[\varepsilon(1-C_\theta)D_{CO2}\nabla\left(\frac{C_{CO2}}{\varepsilon(1-C_\theta)}\right)\right] - Q_{CO2} \quad (5)$$

where C_{CO2} is the CO_2 content in per-unit volume of concrete, ε is the porosity of concrete, D_{CO2} is the diffusion coefficient of CO_2 in concrete gaseous phase, and Q_{CO2} is the sink term representing the consumption rate of CO_2 in concrete during carbonation, which can be approximated as follows [33],

$$\frac{\partial S_{CO2}}{\partial t} = Q_{CO2} = k_{CO2}\left(1-\frac{S_{CO2}}{\bar{S}_{CO2}}\right)C_{CO2} \quad (6)$$

where k_{CO2} is the reaction rate constant, S_{CO2} is the amount of CO_2 consumed during the carbonation, and $\bar{S}_{CO2}$ is the maximum amount of CO_2 that can be consumed by concrete carbonation, which can be expressed as follows [34],

$$\bar{S}_{CO2} = 0.75 \times Cem \times CaO \times \frac{M_{CO2}}{M_{CaO}} \quad (7)$$

where Cem in kg/m^3 is the cement content, CaO is the amount of calcium oxide per weight of cement (for most concrete CaO~0.64), M_{CO2} (=44 g/mol) and M_{CaO} (=56 g/mol) are the molar mass of CO_2 and CaO, respectively. The reduction factor of 0.75 used in Eq.(7) means that not all Cem or all CaO in concrete could be used to consume CO_2 [34]. Note that Eq.(6) holds only when $S_{CO2} \le \bar{S}_{CO2}$; otherwise Q_{CO2}=0. Substituting Eq.(6) into (5), it yields,

$$\frac{\partial C_{CO2}}{\partial t} = \nabla\left[\varepsilon(1-C_\theta)D_{CO2}\nabla\left(\frac{C_{CO2}}{\varepsilon(1-C_\theta)}\right)\right] - k_{CO2}\left(1-\frac{S_{CO2}}{\bar{S}_{CO2}}\right)C_{CO2} \quad (8)$$

For a given concrete Eqs.(6) and (8) can be used to determine the contents of C_{CO2} and S_{CO2} if the initial and boundary conditions of them are defined. Since the carbonation reaction in the present model is assumed to take place only at the carbonation front, the carbonation depth of the concrete can be identified directly by the point where C_{CO2} changes from $C_{CO2} > 0$ to $C_{CO2} = 0$. In other words, the carbonated zone and un-carbonated zone can be defined by $C_{CO2} > 0$ and $C_{CO2} = 0$, respectively.

When a concrete is exposed to a marine environment, chloride ions will transport into the concrete from its surrounding environment. For an unsaturated concrete, the chloride transport in concrete is influenced not only by the moisture transport but also by the carbonation reactions of concrete. The latter is because the carbonated concrete has less chloride binding capacity. In the case where the concrete has already contained both the free and bound chlorides the carbonation can release the bound chloride back to free chloride [35]. Fig.1 depicts the interaction scheme of chloride and carbon dioxide transport in unsaturated concrete. The mass conservation equation of chloride considered in per-unit volume of concrete can be expressed as follows [36,37],

$$\frac{\partial C_T}{\partial t} = -\nabla\left(\varepsilon C_\theta J_{Cl} + C_f D_\theta \nabla C_\theta\right) \quad (9)$$

where C_T is the total chloride content in per-unit volume of concrete and J_{Cl} is the flux of chloride in concrete liquid phase. The total chloride content is the sum of free and bound chlorides (see Fig.1), that is,

$$C_T = C_f + S_p + S_c \quad (10)$$

where C_f is the content of free chloride, S_p and S_c are the contents of physically and chemically

bound chlorides, respectively. The flux of free chloride pass through the unit area of liquid in concrete liquid phase can be expressed as follows [37,38]

$$J_{Cl} = -\frac{D_{Cl}C_f}{C_f+S_p}\nabla\left(\frac{C_f+S_p}{\varepsilon C_\theta}\right) \tag{11}$$

where D_{Cl} is the diffusion coefficient of chloride ions in concrete liquid phase. Substituting Eqs.(10) and (11) into (9), it yields,

$$\frac{\partial C_f}{\partial t} + \frac{\partial S_p}{\partial t} + \frac{\partial S_c}{\partial t} = \nabla\left[\varepsilon C_\theta D_{Cl}\left(\frac{C_f}{C_f+S_p}\right)\nabla\left(\frac{C_f+S_p}{\varepsilon C_\theta}\right) - C_f D_\theta \nabla C_\theta\right] \tag{12}$$

The mass conservation equations of Eqs.(1), (6), (8) and (12) describe the interaction between the transports of chlorides and CO_2 in unsaturated concrete (see Fig.2) and can be used to determine C_θ, C_{CO2}, S_{CO2}, and C_f if the relationship between the free and bound chlorides, that is so-called chloride binding isotherm, is known. Extensive research has been carried out to identify the mechanism of chloride binding in concrete in last three decades. However, most of the work focused on the concrete that is in a saturated state, for example, [39,40,41,42,43,44,45]. Mathematically, the bound chlorides can be divided into physically bound chloride and chemically bound chloride. The former is stacked on the pore surface but still remains its negative charge and thus is similar to the free chloride except for its immovable feature. The latter is due to the chemical reaction between chloride ions and C_3A in cement to form calcium chloroaluminate, which is sometimes referred to as Friedel's salt [35,42]. The chemical binding of chloride ions in concrete is influenced by temperature, pH, moisture content and the type of cement [39,40]. Note that the chemically bound chloride can release when carbonation takes place because of its weak stability [46]. Thus one can use the following first-order reaction equation to calculate the chemically bound chloride,

$$\frac{\partial S_c}{\partial t} = k_{CL}\left(1 - \frac{S_c}{\bar{S}_{CL}}\right)C_f \tag{13}$$

where k_{CL} is the constant representing the chemical binding rate of chloride and $\bar{S}_{CL}$ is the maximum capacity of chemical binding of chlorides in concrete. To reflect the effect of concrete carbonation on the chemical binding capacity, the following equation is assumed for calculating $\bar{S}_{cl}$,

$$\bar{S}_{CL} = \alpha_2 C_f^{\beta_2} C_{fs}^{1-\beta_2}\left(1 - \frac{\gamma S_{CO2}}{\bar{S}_{CO2}}\right) \tag{14}$$

where α_2 and β_2 are the experimentally determined dimensionless constants, C_{fs} is the surface concentration of free chloride, and γ is the constant reflecting the effect of carbonation on the capacity of chemical binding of chlorides. The case of γ=0 implies that the carbonation has no effect on chloride binding; whereas γ=1 means that a fully carbonated concrete has no chemical binding ability. The physically bound chloride is assumed to be an exponent function of free chloride, described using Freundlich isotherm [40] and given by Eq.(15),

$$S_p = \alpha_3 C_f^{\beta_3} C_{fs}^{1-\beta_3} \tag{15}$$

where α_3 and β_3 are the experimentally determined dimensionless constants. Substituting Eqs.(14) and (15) into (12) and (13), it yields,

$$\left(1+\alpha_3\beta_3 C_f^{\beta_3-1}C_{fs}^{1-\beta_3}\right)\frac{\partial C_f}{\partial t}=\nabla\left[\frac{\varepsilon C_\theta D_{Cl}}{1+\alpha_3 C_f^{\beta_3-1}C_{fs}^{1-\beta_3}}\nabla\left(\frac{C_f+\alpha_3 C_f^{\beta_3}C_{fs}^{1-\beta_3}}{\varepsilon C_\theta}\right)-C_f D_\theta \nabla C_\theta\right]$$

$$-k_{CL}\left[1-\frac{S_c}{\alpha_2 C_f^{\beta_2}C_{fs}^{1-\beta_2}\left(1-\frac{\gamma S_{CO2}}{S_{CO2}}\right)}\right]C_f \tag{16}$$

$$\frac{\partial S_c}{\partial t}=k_{CL}\left[1-\frac{S_c}{\alpha_2 C_f^{\beta_2}C_{fs}^{1-\beta_2}\left(1-\frac{\gamma S_{CO2}}{S_{CO2}}\right)}\right]C_f \tag{17}$$

For a given concrete Eqs.(16) and (17) can be used to determine the contents of free chloride C_f and chemically bound chloride S_c if the initial and boundary conditions of them are defined. After the free chloride content is determined, the physically bound chloride can be calculated directly by using Eq.(15), and thus corresponding total chloride content can be evaluated. Note that the governing equations (6) and (8) for describing the transport of CO_2 involve the degree of saturation of concrete; whereas the governing equations (16) and (17) for describing the transport of chlorides involve not only the degree of saturation of concrete but also the level of carbonation, and thus they are all coupled together and need to be solved simultaneously.

3. Solution of coupled transport equations

The above section describes the coupled transport of moisture, carbon dioxide, and chlorides in an unsaturated concrete. It can be seen from the mass conservations of moisture, carbon dioxide, and chlorides shown by Eqs.(1), (6), (8), (16) and (17) that, the governing equation for the moisture, Eq.(1), can be solved independently; while the governing equations for the carbon dioxide and chlorides, Eqs.(6), (8), (16) and (17), have to be solved together as they are coupled each other. The partial differentiation equations of Eqs.(1), (6), (8), (16) and (17) can be solved numerically using an explicit or an implicit time integration scheme [47,48]. By rewriting Eqs.(1), (6), (8), (16), and (17) into the form of matrix, it yields,

$$[\mathbf{M}]\{\dot{\mathbf{C}}\}=[\mathbf{K}]\{\mathbf{C}\}+\{\mathbf{Q}\} \tag{18}$$

where $[\mathbf{M}]$ is the "mass"-type matrix, $[\mathbf{K}]$ is the "stiffness"-type matrix, $\{\mathbf{Q}\}$ is the column vector representing the source term, $\{\mathbf{C}\}$ is the column vector representing the spatial discrete unknowns. From a given vector $\{\mathbf{C}\}_n$ at the time step n, one can solve Eq.(18) for the unknown vector $\{\mathbf{C}\}_{n+1}$ at the time step n+1 as follows,

$$\left(\frac{1}{\Delta t}[\mathbf{M}]-\theta[\mathbf{K}]\right)\{\mathbf{C}\}_{n+1}=\left(\frac{1}{\Delta t}[\mathbf{M}]+(1-\theta)[\mathbf{K}]\right)\{\mathbf{C}\}_n+\{\mathbf{Q}\}_n+\theta(\{\mathbf{Q}\}_{n+1}-\{\mathbf{Q}\}_n) \tag{19}$$

where Δt is the time increment and θ is a constant. The cases of θ=0 and θ=1 represent the explicit and implicit schemes, respectively. Considering the nature of nonlinearity and the involvement of sink terms in the mass conservation equations, the use of the explicit scheme would be more effective, provided that the time increment is chosen to be small enough so that the obtained solutions have no oscillation. In the numerical examples presented in the next section, Eqs.(1), (6), (8), (16) and (17) are all solved using the explicit scheme in which the

derivatives are approximately replaced using finite difference formulas. Fig.3 shows the flowchart of the numerical simulation employed in the present study. Note that the moisture transport generates a convection of chloride ions. Difficulties may arise when numerically solving the convection-diffusion equation where the problem is dominated by the convection [49]. To overcome this kind of numerical difficulties, one should use small element size or small grid or adaptive scheme to achieve stable and convergent solutions [50].

4. Numerical examples

The first numerical example is the simulation of the water absorption of a mortar specimen of size 40×40×20 mm, for which the details of experiments was reported in [51]. The specimen is assumed to have an initial saturation of C_0=0.09 and is immersed into a combined NaOH (1.0 kg/m^3) and KOH (4.65 kg/m^3) solution from its one side, while all other sides are sealed. Fig.4 shows the comparison of the predicted saturation profiles and those measured using gamma-ray attenuation reported in [51]. In the simulation the constants used in Eq.(2) for the moisture diffusivity are assumed as α_1=1.4x10^{-9} m^2/s and β_1=2.25. The boundary conditions employed are assumed as C_0=1 at x=0 and $\partial C_0/\partial x$=0 at x=20 mm. It is evident from Fig.4 that there is very good agreement between the numerically predicted and experimentally obtained profiles. Note that the initial concentrations of ionic species in the mortar specimens were not reported in the experiment and thus the osmotic effect is not considered in the present simulation. For the case of desorption Fig.5 shows the variation of the degree of saturation in the initially saturated mortar (C_0=1) when subjected to a drying process with 10% saturation from its one side (C_0=0.1 at x=0), while all other sides are sealed ($\partial C_0/\partial x$=0 at x=20 mm). It can be seen from the figure that, similar to the saturation process shown in Fig.4, the drying process is also very quick initially and then become slow when time increases.

The second example is the simulation of the concrete carbonation of a 50 mm long cylindrical concrete specimen when subjected to fast carbonation in a carbonation chamber. The specimen simulated has a porosity of ε=0.22 with the degree of saturation C_θ=0.15, and is exposed to 50% CO_2 concentration on its two end sections, while the cylindrical surface is sealed. In the simulation the diffusion coefficient of CO_2 in the gaseous phase and the reaction rate constant are assumed to be D_{CO2}=7.0x10^{-10} m^2/s and k_{CO2}=8.0x10^{-4} 1/s. The maximum amount of CO_2 that can be consumed during the carbonation is assumed to be 10 times of the CO_2 concentration on the exposed surface. The initial and boundary conditions used in the simulation are assumed as C_{CO2}=S_{CO2}=0 at t=0; C_{CO2}=0.5x1.225x0.85ε kg/m^3, where 0.5 represents 50% CO_2 concentration, 1.225 in kg/m^3 is the density of the 50% CO_2 gas applied on the exposed surface, and 0.85ε is the volume fraction of gaseous phase on the exposed surface, and S_{CO2}=$\bar{S}_{CO2}$=10C_{CO2} at x=0, and $\partial C_{CO2}/\partial x$=$\partial S_{CO2}/\partial x$=0 at x=25 mm, respectively. Fig.6 shows the concentration profiles of CO_2 at 2, 8 and 20 days, respectively, obtained by solving Eqs.(6) and (8) numerically. For the purpose of comparison, the results reported in literature [52] are also superimposed in the figure, where the experimental results were obtained by using accelerated carbonation tests of concrete [52,53]. It can be seen from the figure that CO_2 moves quickly in the beginning but decreases with increased time. The concentration profile of CO_2 can be generally characterised by a linear line from the exposed surface followed by a smooth

curve near the carbonation front. This is attributed to the fast consumption of CO_2 during the carbonation. Fig.7 shows the depth-time curves obtained from the present simulation and the published experimental results [52,53]. It is evident from the figure that there is a good agreement between the simulation and experimental results. Both of them are very close to the theoretical curve of the depth to the square root of time.

The third example is the simulation of the salt ponding tests of chloride diffusion in mortars mixed with water-to-cement ratio 0.45 (M45) and cement-to-sand ratio 0.453. In the experiments the mortar specimens of cylindrical type sealed on the cylindrical surface and one of the two end surfaces were immersed into 3.0% NaCl solution (equivalent to 0.52 mole/l chloride concentration). The details of the experiments are reported in ref. [54]. Fig.8 shows the comparison of the total chloride profiles at three different exposure times obtained from the numerical simulations and experimental tests (M45). In the simulation the porosity, density and saturation of the mortar are assumed to be ε=0.18 (for water-to-cement ratio 0.45), ρ_m=2162 kg/m^3, and C_θ=1.0, respectively. The initial and boundary conditions for the free chloride and chemically bound chloride are assumed as C_f=S_c=0 at t=0; C_f=0.52x35.45xε=3.32 kg/m^3, where 0.52 is the mole/l concentration of chlorides applied on the exposed surface and 35.45 is the molar mass of chloride, and S_c=0.569xC_f=1.89 kg/m^3, where 0.569 is the assumed ratio between the chemically bound chloride and free chloride at the exposed surface, at x=0 and $\partial C_f/\partial x$=$\partial S_c/\partial x$=0 at x=50 mm, respectively. The chloride diffusion coefficient in the mortar is taken as D_{cl}=3.15x10^{-11} m^2/s. The parameters used for chloride binding are α_2=0.087, β_2=0, γ=1.0, α_3=1.11, β_3=1.0 and k_{cl}=2.5x10^{-6} 1/s. It can be seen from the figure that the predicted total chlorides are in good agreement with the experimental data for all three times. If a pure diffusion model is used, a time-dependent chloride diffusion coefficient has to be used in order to fit the experimental data at different exposure times. Fig.9 shows the profiles of the free chloride, physically and chemically bound chlorides at the time of 5-month exposure together with the experimentally measured total chloride profile. The figure demonstrates that the majority of chlorides transported into the mortar were bound to the solid phase of the mortar, indicating that the consideration of chloride binding in cementitious materials is extremely important.

The fourth example is the simulation of the site tests of mortars mixed with water-to-cement ratio 0.4 and cement-to-sand ratio 0.556. In the tests the mortar specimens of cylindrical type sealed on the cylindrical surface and one of the two end surfaces were exposed to the tidal zone with a daily drying-wetting-drying cycle of approximately 10-4-10 (hours). The details of the experiments are reported in ref. [55]. In the present simulation the porosity and density of the mortar are assumed to be ε=0.15 and ρ_m=2240 kg/m^3 (for water-to-cement ratio 0.4). The CO_2 concentration in the surrounding air is 5%. The chloride concentration in the surrounding seawater is 19.4 g/l (equivalent to 0.547 mole/l chloride concentration). The initial conditions used are assumed as C_θ=1.0, C_{CO2}=S_{CO2}=0, and C_f=S_c=0. The boundary conditions at the exposed surface (x=0) are assumed as follows,

$$C_\theta(t,0) = 0.6117 + 0.4113\sum_1^4 \frac{1}{k\pi}\left[\sin\frac{7k\pi}{6} - \sin\frac{5k\pi}{6}\right]\cos\frac{2k\pi t}{24\times60\times60} \quad (20)$$

$$C_{CO2}(t,0) = 0.05 \times 1.225\varepsilon(1 - C_\theta)\ \ (\text{kg/m}^3) \quad (21)$$

$$\frac{\partial S_{CO2}(t,0)}{\partial x} = 0 \quad (22)$$

$$C_f(t,0) = 1.3 \times 19.4\varepsilon C_\theta \ \ (\text{kg/m}^3) \quad (23)$$

$$\frac{\partial S_c(t,0)}{\partial x} = 0 \quad (24)$$

where Eq.(20) is a period function of time to represent the daily drying-wetting-drying cycle. The pre-factor of 1.3 used in Eq.(23) reflects the effect of accumulation of chloride on the exposed surface caused by the drying period. Fig.10 graphically shows the variation of C_θ, C_{CO2} and C_f on the exposed surface (x=0) with the time. Note that during the drying period the surface saturation of the specimens is assumed to remain around 0.5 because of the high humidity in the tidal environment. Zero fluxes for C_θ, C_{CO2}, S_{CO2}, C_f and S_c are assumed at the boundary (x=50 mm) where the surface is sealed. Other parametric values used in the simulation are: α_1=5.5x10^{-10} m^2/s, β_1=2.25, D_{CO2}=3.5x10^{-10} m^2/s, k_{CO2}=8.0x10^{-4} 1/s, $\bar{S}_{CO2}$=5x1.225ε kg/m^3, D_{Cl}=7.5x10^{-12} m^2/s, k_{Cl}=2.5x10^{-5} 1/s, α_2=0.4, β_2=0, α_3=0.4, β_3=1.0, γ=1.0. It should be stressed here that the surface free chloride concentration varies with time during the drying-wetting-drying cycles as indicated by Eq.(23). This is due to the variation of the surface saturation since C_f is defined as the free chloride in per unit of concrete rather than in per unit of pore solution. Fig.11 shows the distribution profiles of the saturation, CO_2 and chloride contents in the mortar specimens after they have had exposure for one, four and eight weeks. It can be seen from Fig.11a that, after eight-week exposure the initially saturated specimen becomes stabilised. The subsequent wetting will increase its saturation at a certain degree but will return to the stabilised state after the specimen is dried again. This is because the drying period is much longer than the wetting period. Fig.11b shows that the process of diffusion of CO_2 decreases with the increase of time. This is due to the consumption of CO_2 during the carbonation. Fig.11c shows the profiles of total chlorides. It can be seen from the figure that the total chloride exhibits an initial increase from the exposed surface followed by a decrease with increased depth. The peak point of the profile is a little bit away from the exposed surface and moves inwards slowly with increased time. Fig.11d shows the profiles of the sum of the free and physically bound chlorides. The difference between Fig.11c and Fig.11d thus reflects the chemically bound chloride. It can be observed from Fig.11d that the variation feature of the chloride profiles with the depth is similar to that shown in Fig.11c, except that the overall concentrations shown in Fig.11d are slightly smaller than those shown in Fig.11c, reflecting the effect of chemically bound chloride. The main reason that the highest chloride concentration in the profile does not occur at the exposed surface but is inside the outer surface is due to the combined action of moisture convection during the wetting-drying-wetting cycles and the release of chemically bound chloride in the carbonation zone. It is noticed that the chloride concentration at the peak point increases with the time. For example, the total chloride content (wt % of mortar mass) at the peak pint shown in Fig.11c is 0.25 at week 1, 0.30 at week 4, and 0.34 at week 8, whereas the total chloride content at the exposed surface for a fully saturated state calculated from the boundary condition is about 0.304. Similarly, the sum of free and physically bound chlorides (wt % of mortar mass) at the peak pint shown in Fig.11d is 0.17 at week 1, 0.22 at week 4, and 0.28 at week 8, whereas the sum of free and physically chlorides at the exposed surface for a fully saturated state calculated from the boundary condition is about 0.237. This reflects the importance of considering moisture convection when modelling chloride transport in

unsaturated concrete. Comparing the profiles of CO_2 shown in Fig.11b and those of chlorides shown in Fig.11c or Fig.11d, one can find that the moisture convection speeds up the transport of chlorides but slows down the transport of CO_2.

To demonstrate the present model, Fig.12 shows the comparison of the chloride profiles obtained from the present simulation and those measured in the site tests. In the site tests the chlorides were measured using powder samples to determine their water-soluble chloride concentration, which represents the sum of free and physically bound chlorides. It is evident from Fig.12 that there is a good agreement between the simulations and experiments. The marginal difference between them could be due to the random weather conditions in the testing site and the difference of sampling times (e.g. samples were taken during the wetting or drying period). Note that in the present model the physically bound chloride is assumed to be linearly proportional to the free chloride, thus it is not only the total chloride profile but also the free chloride profile that has a maximum concentration at the inner concrete rather than at the exposed surface.

To explain the importance of considering chemically bound chloride and the effect of concrete carbonation on the evolution of chemically bound chloride, Fig.13 shows the comparisons of the free and total chloride profiles obtained from the present model and those obtained from the traditional transport model in which the chloride binding is taken into account by using a Freundlich isotherm, which is similar to a special case of the present model when both k_{CL} and S_c are zero. It can be seen from Fig.13a that the free chlorides in the convection zone given by the two models are very close. This is because the chemically bound chloride has been released in the convection zone and thus there is almost no difference between the two models. However, in the inner diffusion zone behind the peak point, the free chloride predicted by the present model is lower than that predicted by the traditional transport model. This is mainly due to the effect of chemically bound chloride considered in the present model. However, in terms of the total chloride shown in Fig.13b, the concentration predicted by the present model is generally higher than that predicted by the traditional transport model. Only exception is in the deep inner region near the diffusion front where the concentration predicted by the present model is lower. The former is due to the contribution of chemically bound chloride involved in the present model; whereas the latter is due to the faster diffusion of chloride when the chemical binding of chlorides is ignored in the traditional transport model. The results shown in Fig.13 indicate that the convection zone near the exposed surface where the chloride concentration increases with the depth is mainly due to the surface drying which reduces the free chloride content in per unit volume of concrete and causes the convection and diffusion of chlorides in an opposite direction, although the release of chemically bound chloride in the convection zone could also affect the chloride concentration at the peak point.

5. Conclusions

This paper has presented a coupled transport model of moisture, carbon dioxide and chloride in unsaturated concrete exposed to wetting and drying cycles. The model considers not only the diffusion and convection of individual components but also the concrete carbonation, chloride

binding and the effect of concrete carbonation on chloride binding capacity. The model has been applied to simulate the moisture absorption and desorption of concrete, concrete carbonation in partially saturated concrete, chloride transport in saturated and unsaturated concretes when subjected to wetting and drying cycles. The model has been validated by using published experimental data for various different cases. From the results obtained, the following conclusions can be drawn.

- The moisture flow generated during wetting and drying cycles has a great impact on the transports of carbon dioxide and chloride in concrete. Thus, it is important to know the exact time-dependent condition of the moisture on the exposed surface during the period of wetting and drying cycles in order to predict the transport behaviour of moisture, carbon dioxide and chloride in concrete.
- The moisture convection during the wetting and drying cycles generally speeds up the transport of chloride from exposed surface to inner concrete but slows down the transport of carbon dioxide from exposed surface into inner concrete. This explains why the carbonation depth is much thinner than the chloride penetration depth.
- The present model has demonstrated that, under the combined actions of the moisture convection due to wetting and drying cycles and the release of chemically bound chloride in carbonation zone the maximum concentration not only in total chloride profile but also in free chloride profile occurs at the inner concrete instead of at the exposed surface as shown in the immersed tests of chloride diffusion.
- The chloride concentration at the peak point in either the total chloride profile or the free chloride profile increases with the increased number of wetting and drying cycles. With the increase of time, the peak value could be greater than the surface chloride value in a fully saturated state.
- To be able to consider the release of bound chloride caused by concrete carbonation, it appears necessary to split the bound chloride into the physically and chemically bound chlorides. Only chemically bound chloride could be released by carbonation.

Acknowledgements - The authors would like to acknowledge the financial support received from the National Natural Science Foundation of China (Grant No. 51978406, 51520105012, 52078300, 52078301).

Declaration of interests - The authors declare that they have no known competing financial interests or personal relationships that could have appeared to influence the work reported in this paper.

References

[1] Sergi, G., Yu, S.W., Page, C.L. Diffusion of chloride and hydroxyl ions in cementitious materials exposed to a saline environment. Magazine of Concrete Research (1992) **44**(158): 63-69.

[2] Dhir, R.K., Jones, M.R., Ng, S.L.D. Prediction of total chloride content profile and concentration/time-dependent diffusion coefficients for concrete. Magazine of Concrete Research (1998) **50**(1): 37-48.

[3] Andrade, C., Climent, M.A., Vera, G.D. Procedure for calculating the chloride diffusion coefficient and surface concentration from a profile having a maximum beyond the concrete surface. Materials and Structures (2015) **48**(4): 863-869.
[4] Saetta, A., Scotta, R., Vitaliani, R. Analysis of chloride diffusion into partially saturated concrete. ACI Materials Journal (1993) **90**(5): 441–451.
[5] Andrade, C., DíEz, J.M., Alonso, C. Mathematical modeling of a concrete surface "skin effect" on diffusion in chloride contaminated media. Adv. Cem. Based Mater. (1997) **6**(2): 39-44.
[6] Hong, K., Hooton, R.D. Effects of cyclic chloride exposure on penetration of concrete cover. Cem. Concr. Res. (1999) **29**(9): 1379-1386.
[7] Wang, Y., Li, L.Y., Page, C.L. Modelling of chloride ingress into concrete from a saline environment. Building and Environment (2005) **40**(12): 1573–1582.
[8] Wang, C.K., Gao, X.J., Zhao, Y.X., Jin, W.L., Xu, Q.L. Peak value distribution of surface chloride concentration and convection depth of concrete. Chin. Ceram. Soc. (2010) **29**(2): 262-267.
[9] Zhang, Y., Jin, W.-L. Distribution of chloride accumulation in marine tidal zone along altitude. ACI Materials Journal (2011) **108**(5): 467-475.
[10] Xu, G., Xu, K., Su, Y., Wang, Y. Transport characteristics of chloride ion in concrete under dry-wet cycles. Journal of Building Materials (2014) **17**(1): 54-59.
[11] Arya, C., Bioubakhsh, S., Vassie, P. Modelling chloride penetration in concrete subjected to cyclic wetting and drying. Magazine of Concrete Research (2014) **66**(7): 364-376.
[12] Arya, C., Vassie, P., Bioubakhsh, S. Chloride penetration in concrete subject to wet/dry cycling: Influence of moisture content. Proceedings of the Institution of Civil Engineers: Structures and Buildings (2014) **167**(2): 94-107.
[13] Gang, X., Yun-Pan, L., Yi-Biao, S., Ke, X. Chloride ion transport mechanism in concrete due to wetting and drying cycles. Structural Concrete (2015) **16**(2): 289-296.
[14] Guan, B.W., Yang, T., Yang, X.K., Xiong, R., Wang, Y.W., Sheng, Y.P. Numerical simulation of chloride ion migration of cement concrete under dry-wet cycles. Materials Research Innovations (2015) **19**(10): 139-143.
[15] Lu, C.-H., Gao, Y., Cui, Z.-W., Liu, R.-G. Experimental analysis of chloride penetration into concrete subjected to drying-wetting cycles. J. Mater. Civil Eng. (2015) **27**(12): 04015036.
[16] Yu, Z.W., Chen, Y., Liu, P., Wang, W.L. Accelerated simulation of chloride ingress into concrete under drying–wetting alternation condition chloride environment. Constr. Build. Mater. (2015) **93**: 205-213.
[17] Lu, C.-H., Li, H., Liu, R.-G. Chloride transport in cracked RC beams under dry-wet cycles. Magazine of Concrete Research (2017) **69**(9): 453-466.
[18] Gao, Y.H., Zhang, J.Z., Zhang, S., Zhang, Y.R. Probability distribution of convection zone depth of chloride in concrete in a marine tidal environment. Constr. Build. Mater. (2017) **140**: 485-495.
[19] Zhang, Y.-R., Zhuang, H.-X., Shi, J.-L., Huang, J., Zhang, J.-Z. Time-dependent characteristic and similarity of chloride diffusivity in concrete. Mag. Concrete Res. (2018) **70**(3): 129-137.
[20] Zhang, Y.-R., Zhang, Y., Huang, J., Zhuang, H.-X., Zhang, J.-Z. Time-dependence and

similarity analysis of peak value of chloride concentration of concrete under the simulated chloride envronment. Constr. Build. Mater. (2018) **181**: 609-617.
[21] Petcherdchoo, A. Closed-form solutions for modeling chloride transport in unsaturated concrete under wet-dry cycles of chloride attack. Construction and Building Materials (2018) **176:** 638-651.
[22] Shen, X.-H., Jiang, W.-Q., Hou, D.-H., Hu, Z., Yang, J., Liu, Q.-F. Numerical study of carbonation and its effect on chloride binding in concrete. Cement and Concrete Composites (2019) **104**: 103402.
[23] Li, K., Zhao, F., Zhang, Y. Influence of carbonation on the chloride ingress into concrete: Theoretical analysis and application to durability design. Cement and Concrete Research (2019) **123**: 105788.
[24] Shen X.-H., Liu, Q.-F., Hu, Z., Jiang W.-Q., Lin, X., Hou, D., Hao, P. Combine ingress of chloride and carbonation in marine-exposed concrete under unsaturated environment: A numerical study. Ocean Engineering (2019) **189**:106350.
[25] Liang, C.-F., Ma, H.-W., Pan, Y.-Q., Ma, Z.-M., Duan, Z.-H., He, Z.-H. Chloride permeability and the caused steel corrosion in the concrete with carbonated recycled aggregate. Construction and Building Materials (2019) **218**: 506-518.
[26] AL-Ameeri, A.S., Rafiq, M.I., Tsioulou, O. Combined impact of carbonation and crack width on the chloride penetration and corrosion resistance of concrete structures. Cement and Concrete Composites (2021) **115**: 103819.
[27] Dang, V.Q., Ogawa, Y., Bui, P.T., Kawai, K. Effects of chloride ions on the durability and mechanical properties of sea sand concrete incorporating supplementary cementitious materials under an accelerated carbonation condition. Construction and Building Materials (2021) **274**: 122016.
[28] Li, D.W, Li, L.Y., Wang, X.F., Xing, F. A double-porosity model for water flow in unsaturated concrete. Applied Mathematical Modelling (2018) **53**: 510-522.
[29] Zhang, Q. Mathematical modelling and numerical study of carbonation in porous concrete materials. Applied Mathematics and Computation (2016) **281**: 16-27.
[30] Bary, B., Sellier, A. Coupled-carbon dioxide-calcium transfer model for carbonation of concrete. Cement and Concrte Research (2004) **34**(10): 1859-1872.
[31] Papadakis, V.G., Vayena, C.G., Fardis, M.N. Fundamental modelling and experimental investigation of concrete carbonation. ACI Materials Journal (1991) **88**(4): 363-373.
[32] Papadakis, V.G., Vayena, C.G., Fardis, M.N. Physical and chemical characteristics affecting the durability of concrete. ACI Materials Journal (1991) **88**(2): 186-196.
[33] Li, D.W., Li, L.Y., Wang, X.F. Mathematical modelling of concrete carbonation with moving boundary. International Communications in Heat and Mass Transfer (2020) **117**:104809.
[34] Pade, C., Guimaraes, M. The CO2 uptake of concrete in a 100 year perspective. Cement and Concrete Research (2007) 37(9): 1348-1356.
[35] Geng, J., Easterbrook, D., Liu, Q.F., Li, L.Y. Effect of carbonation on release of bound chlorides in chloride-contaminated concrete. Magazine of Concrete Research (2016) **68**(7): 353-363.
[36] Geng, J., Li, L.-Y., Wang, Y. Modelling of chloride penetration in unsaturated concrete. Advances in Cement Research (2016) **28**(1): 51-61.

[37] Li, D.W., Li, L.Y., Wang, X.F. Chloride diffusion model in concrete in marine environment with considering binding effect. Marine Structures (2019) **66**: 44–51.
[38] Li, D.W., Wang X.F., Li, L.Y. An analytical solution for chloride diffusion in concrete with considering binding effect. Ocean Engineering (2019) **191**: 106549.
[39] Baroghel-Bouny, V., Wang, X., Thiery, M., Saillio, M., Barberon, F. Prediction of chloride binding isotherms of cementitious materials by analytical model or numerical inverse analysis. Cement and Concrete Research (2012) **42**(9): 1207-1224.
[40] Tang, L.P., Nilsson, L.O. Chloride binding capacity and binding isotherms of OPC pastes and mortars. Cement and Concrete Research (1993) **23**(2): 247-253.
[41] Liu, J., Xing, F., Dong, B.Q., Ma, H.Y., Pan, D. New equation for description of chloride ions diffusion in concrete under shallow immersion condition. Mater. Res. Innov. (2014) **18**(2): 252-265.
[42] Wang, Y., Nanukuttan, S., Bai, Y., Basheer, P.A.M. Influence of combined carbonation and chloride ingress regimes on rate of ingress and redistribution of chlorides in concretes. Construction and Building Materials (2017) **140**: 173-183.
[43] Dhir, R.K., Jones, M.R., McCarthy, M.J. PFA concrete: Chloride ingress and corrosion in carbonated cover. Proceedings of the Institution of Civil Engineers: Structures and Buildings (1993) **99**(2): 167-172.
[44] Ngala, V.T., Page, C.L. Effects of carbonation on pore structure and diffusional properties of hydrated cement pastes. Cement and Concrete Research (1997) **27**(7): 95-1007.
[45] Yuan, C., Niu, D., Luo, D. Effect of carbonation on chloride diffusion in fly ash concrete. Disaster Advances (2012) **5**(4): 433-436.
[46] Geng, J., Easterbrook, D., Li, L.Y., Mo, L.W. The stability of bound chlorides in cement paste with sulfate attack. Cement and Concrete Research (2015) **68**: 211–222.
[47] Li, L.Y., Page, C.L. Finite element modelling of chloride removal from concrete by electrochemical method. Corrosion Science (2000) **42**(12): 2145-2165.
[48] Li, L.Y., Easterbrook, D., Xia, J., Jin, W.L. Numerical simulation of chloride penetration in concrete in rapid chloride migration tests. Cement and Concrete Composites (2015) **63**: 113-121.
[49] Zienkiewicz, O.C., Taylor, R.L. Finite Element Method, Volume 3, Fluid Dynamics (4th edition), Butterworth Heinemann, 2000, Oxford, UK.
[50] Li, L.Y., Bettess, P., Bull, J., Bond, T., Applegarth, I. Theoretical formulations for adaptive finite element computations, Communications in Numerical Methods in Engineering (1995) **11**(10): 857-868.
[51] Baroghel-Bouny,V., Thiéry, M., Wang, X. Modelling of isothermal coupled moisture–ion transport in cementitious materials. Cement and Concrete Research (2011) **41**: 828–841.
[52] Peter, M.A., Muntean, A., Meier, S.A., Böhm, M. Competition of several carbonation reactions in concrete: A parametric study. Cement and Concrete Research (2008) **38**(12): 1385–1393.
[53] Papadakis, V.G., Vayenas, C.G., Fardis, M.N. A reaction engineering approach to the problem of concrete carbonation. AIChE Journal (1989) **35**(10): 1639–1650.
[54] Chen, Y.S., Li, M.C., Chan, Y.W., Yang, C.C. The relationship between accelerated migration time in ACMT and ponding time in ponding test for cement-based materials. Journal of Marine Science and Technology (2012) **20**(1): 1-8.

[55] Wang, Y.Z., Wu, L.J., Wang, Y.C., Li, Q.M., Xiao Z. Prediction model of long-term chloride diffusion into plain concrete considering the effect of the heterogeneity of materials exposed to marine tidal zone. Construction and Building Materials (2018) **159**: 297–315.

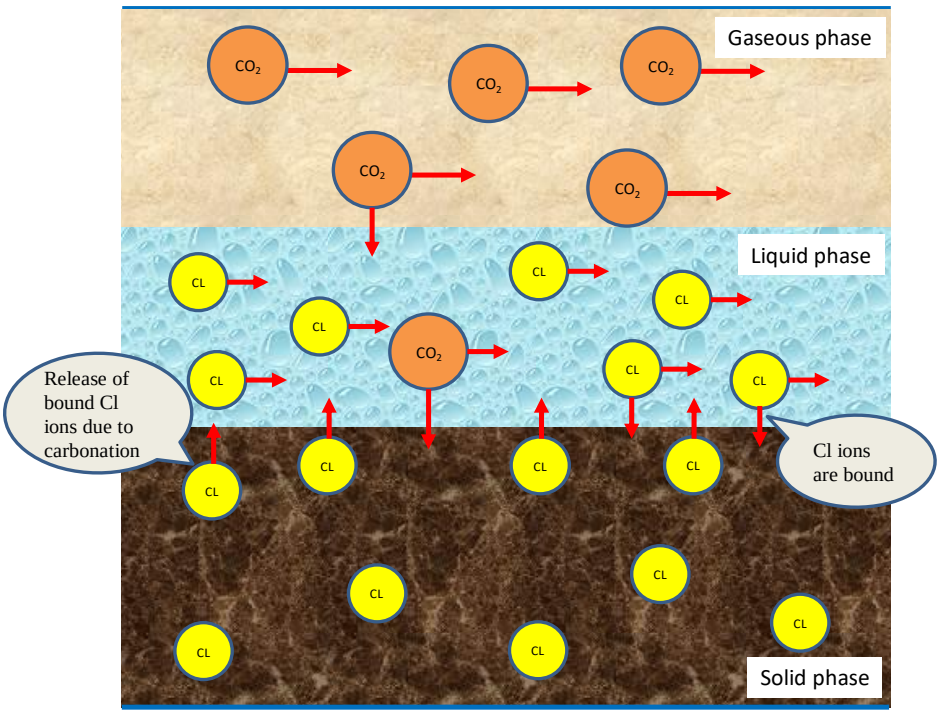

Fig.1 Scheme representing interaction of chloride (Cl) and carbon dioxide (CO_2) transport in an unsaturated three-phase concrete.

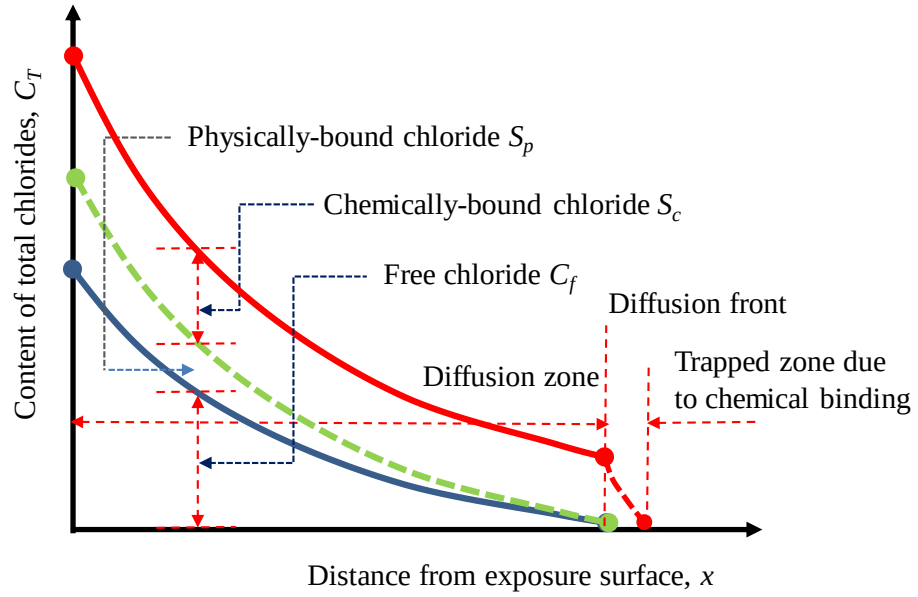

(a)

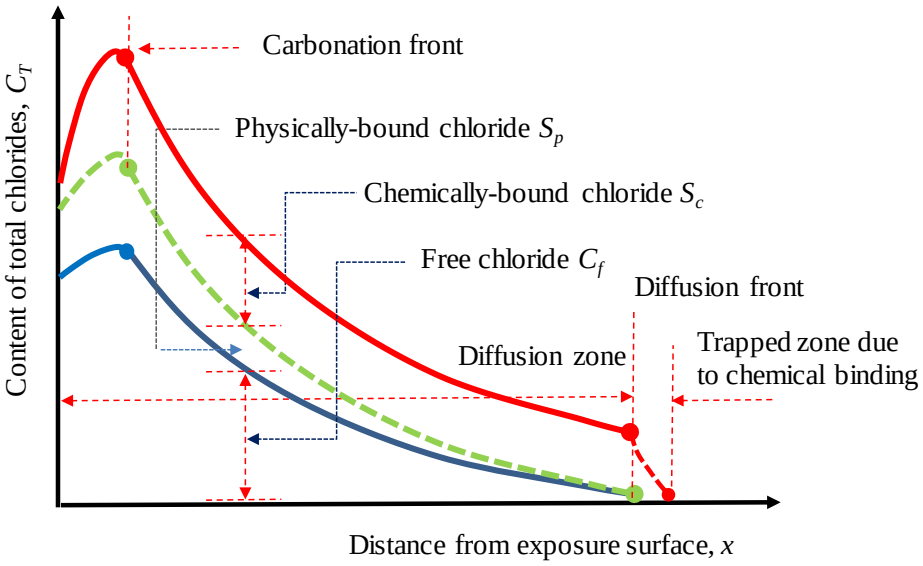

(b)

Fig.2. Schematic distribution profiles of free, physically and chemically bound chlorides in (a) uncarbonated and (b) partially carbonated concrete.

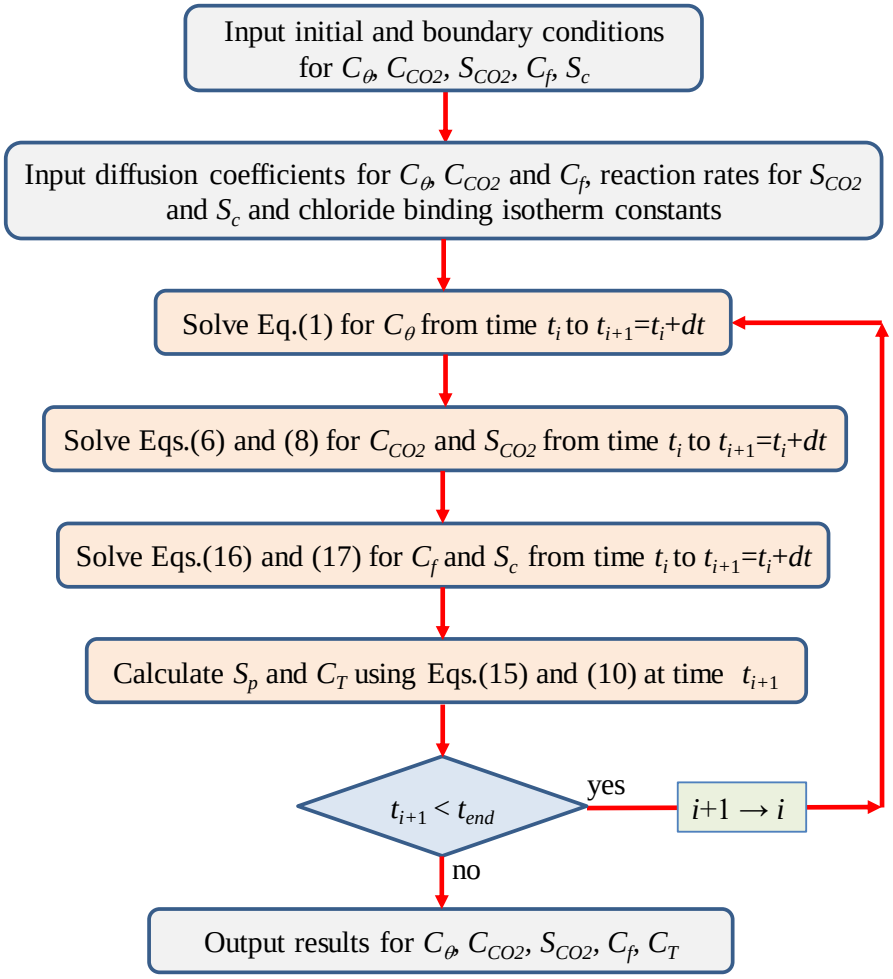

Fig.3 Flowchart of numerical simulation of coupled transport of moisture, carbon dioxide, and chloride ions in non-saturated concrete.

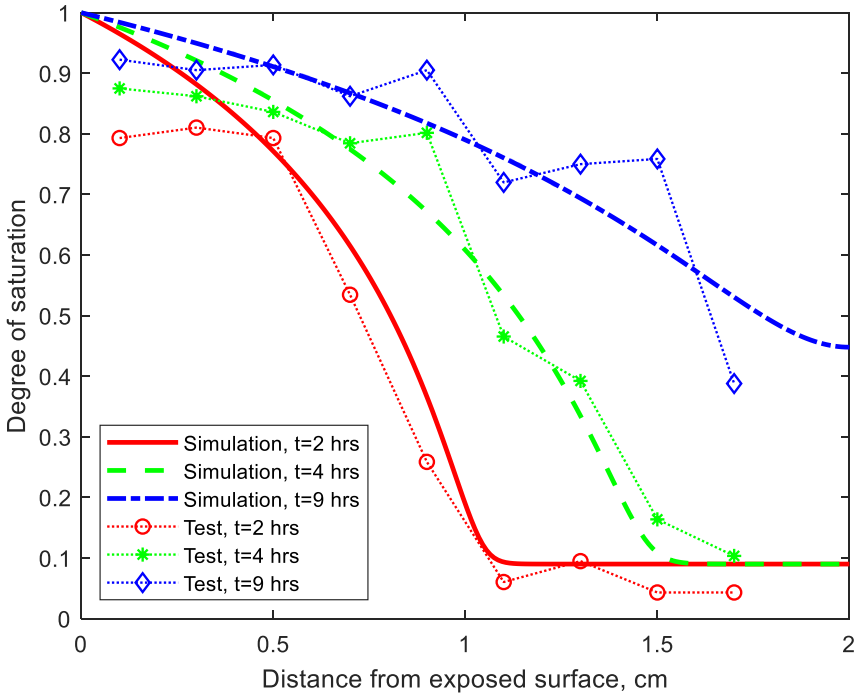

Fig.4 Comparison of simulated and measured saturation profiles during water absorption of mortar specimens (test data were from [51]).

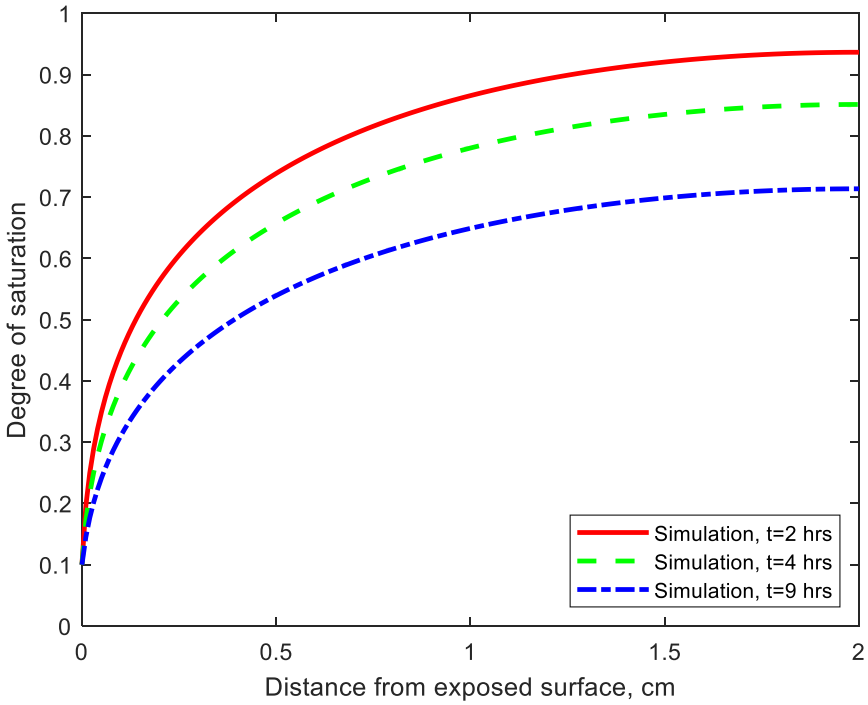

Fig.5 Saturation profiles during drying process of initially saturated mortar specimens.

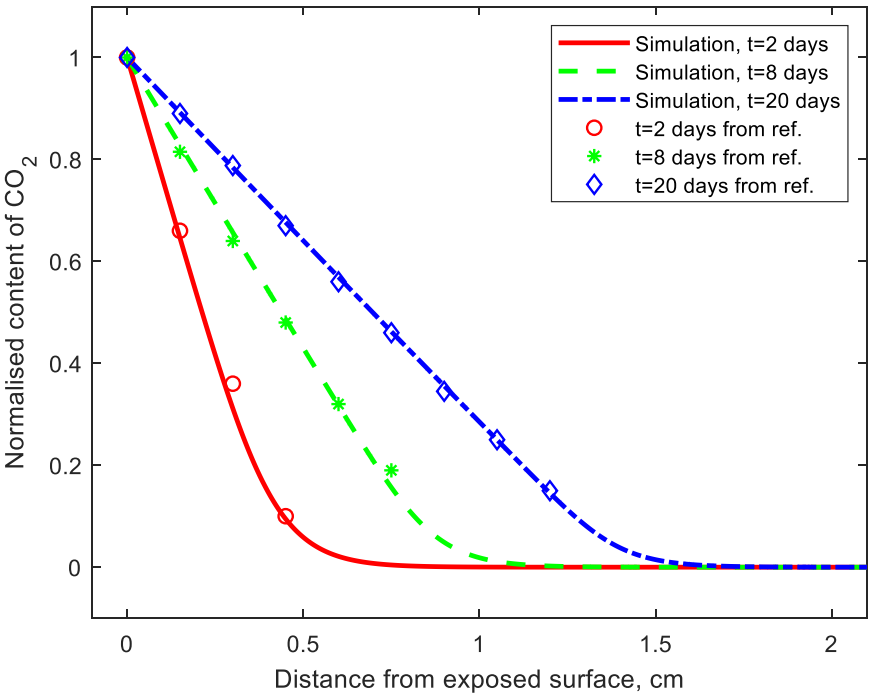

Fig.6 Concentration distribution profiles of CO_2 at different times for concrete exposed to 50% CO2 in carbonation chamber (results given by dots are taken from ref. [52]).

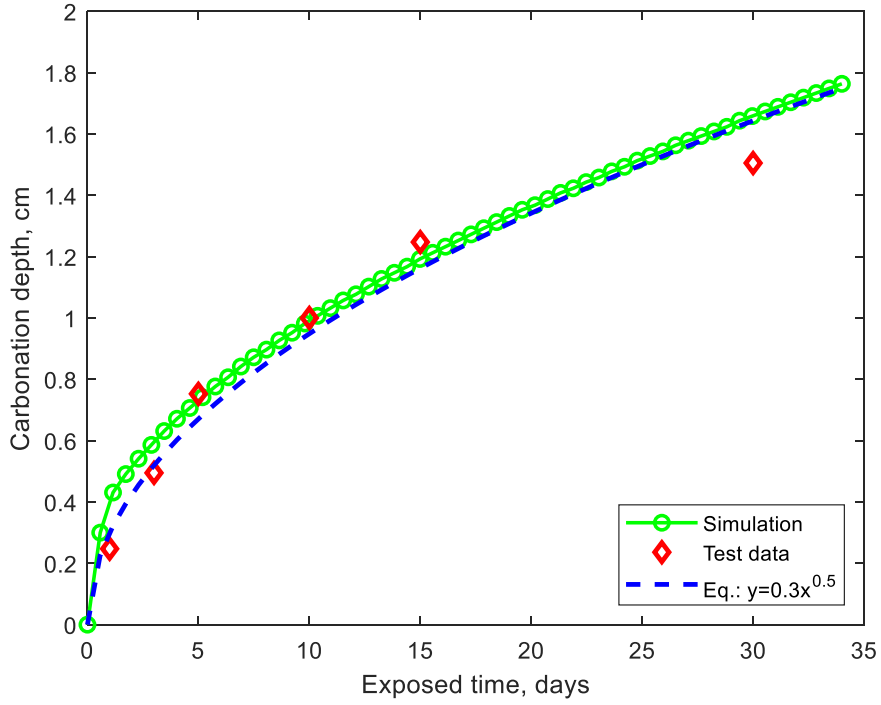

Fig.7 Comparison of simulated and measured carbonation depths (test data from ref. [52,53]).

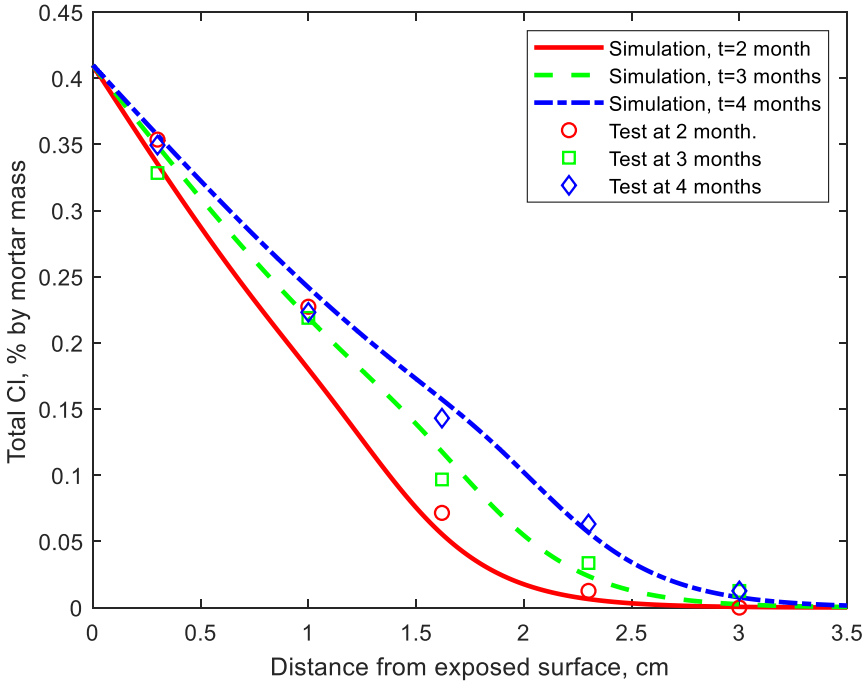

Fig.8 Comparison of simulated and measured total chlorides at the times of 2-, 3- and 4-month exposure (test data from ref. [54]).

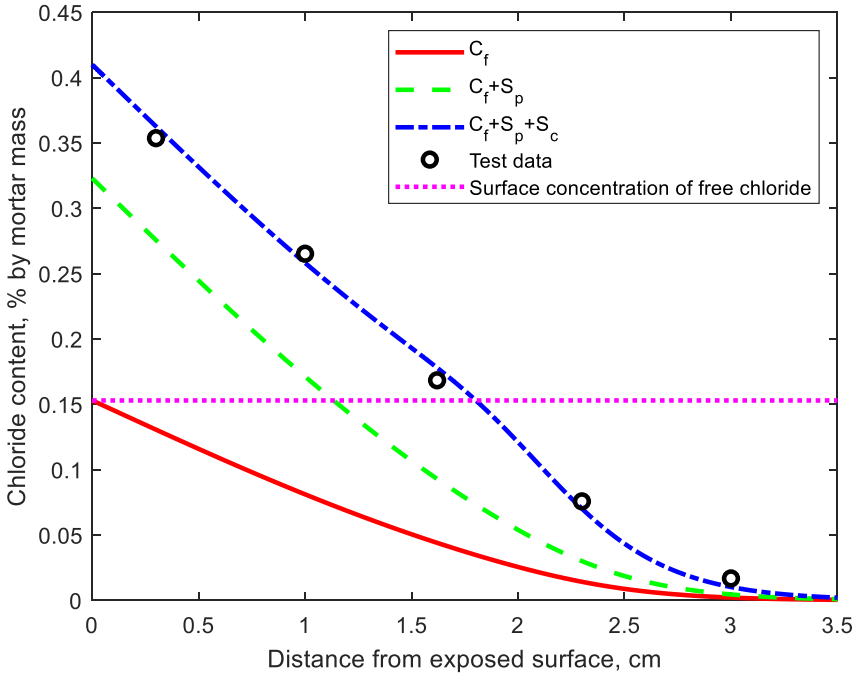

Fig.9 Comparison of simulated and measured total chlorides at the time of 5-month exposure (test data from ref. [54]).

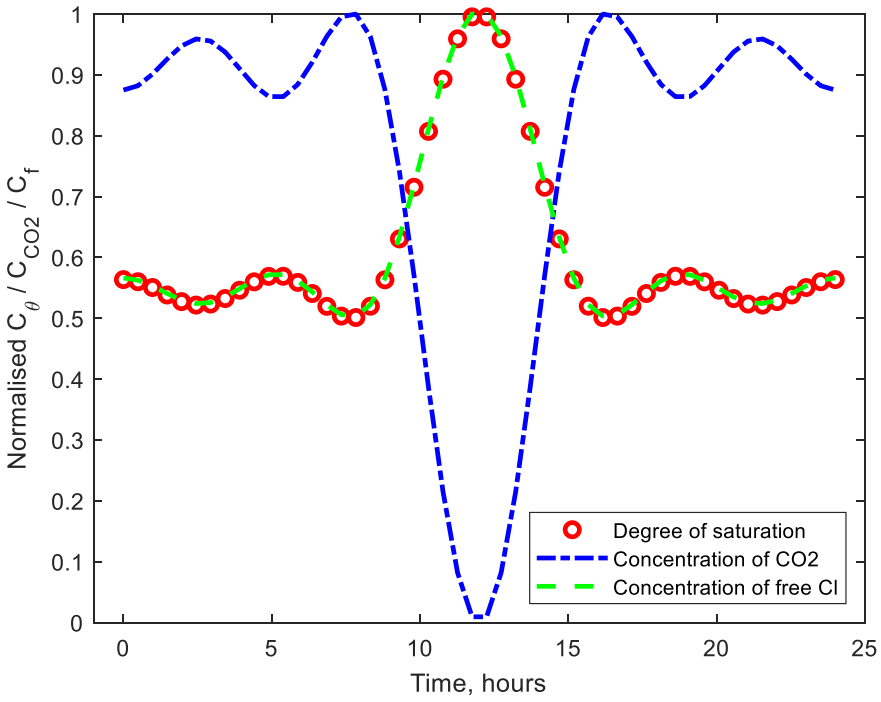

Fig.10 Variation of saturation, CO_2 and free chloride on exposed surface of tested specimens.

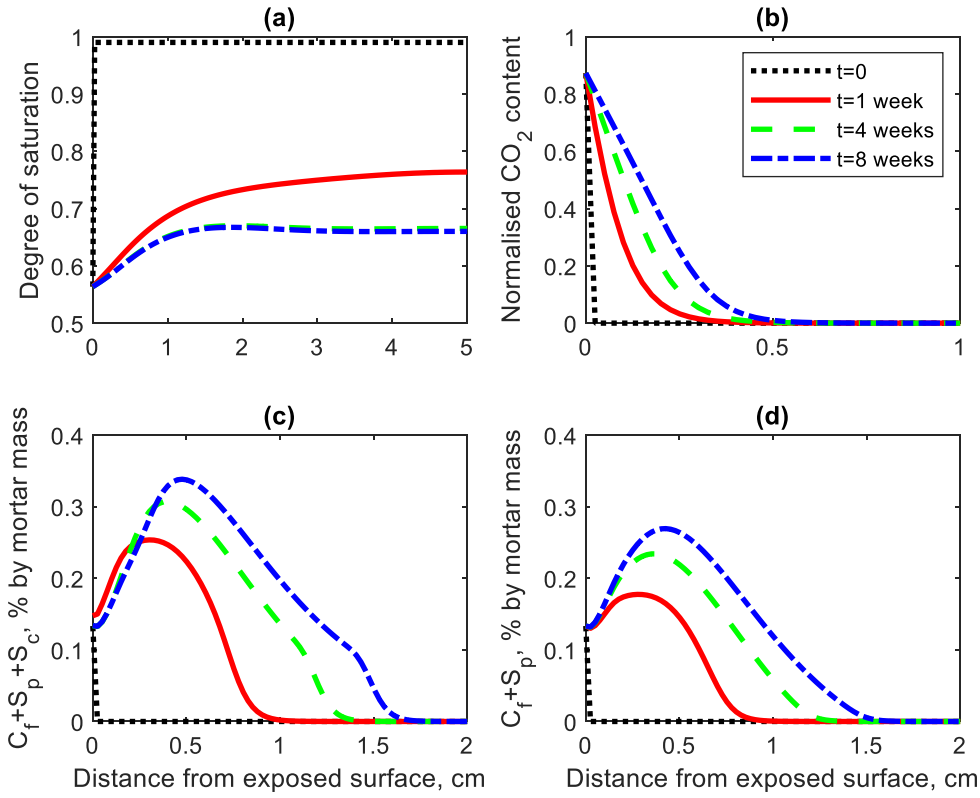

Fig.11 Concentration profiles of saturation, CO_2, and chlorides at different exposure times.

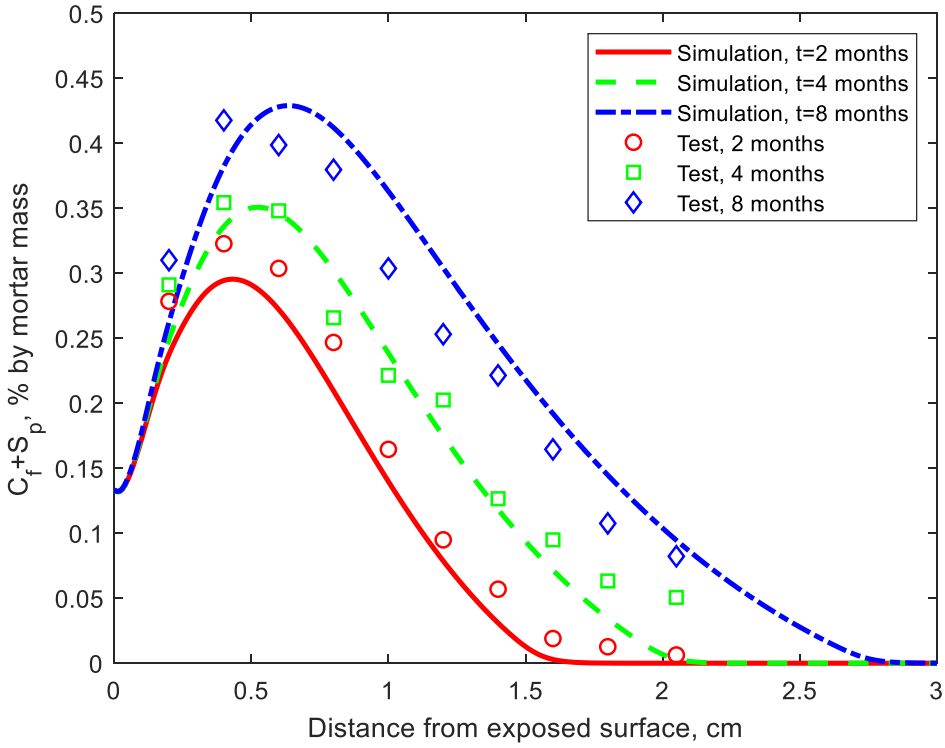

Fig.12 Comparison of chloride profiles between simulation and test (test data from ref. [55]).

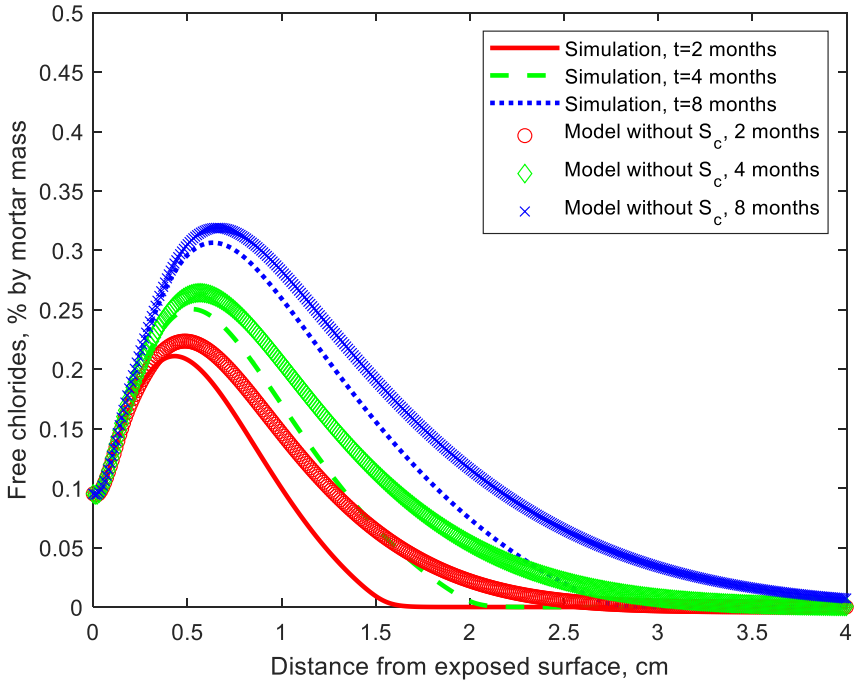

(a)

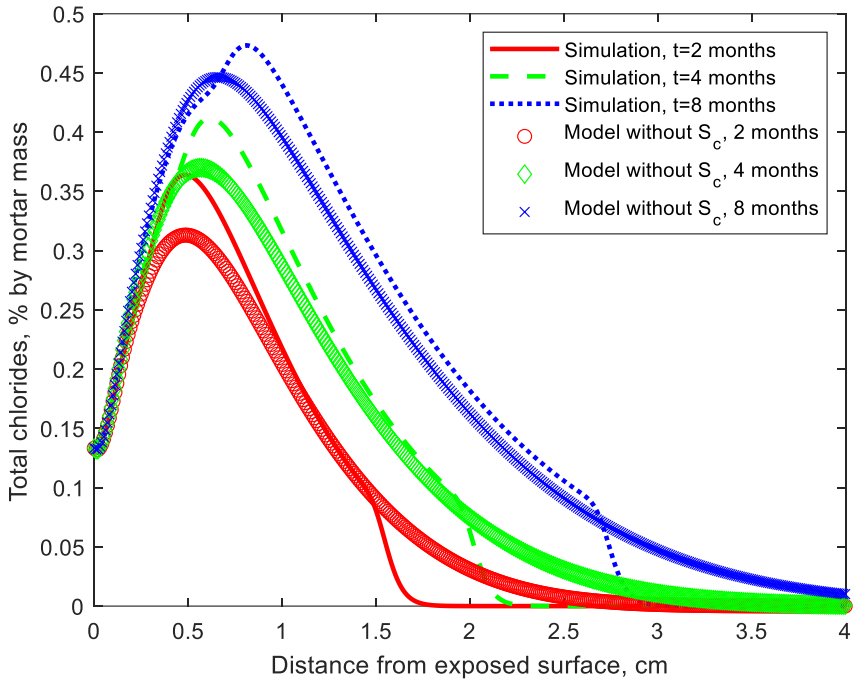

(b)

Fig.13 Comparison of chloride profiles between present model and physically bound chloride model (S_c=0 and k_{CL}=0). (a) Free chlorides and (b) total chlorides.